ISSN 0021-3640, JETP Letters, 2010, Vol. 92, No. 9, pp. 575–579. © Pleiades Publishing, Inc., 2010.
Original Russian Text © P.P. Vabishchevich, V.O. Bessonov, F.Yu. Sychev, M.R. Shcherbakov, T.V. Dolgova, A.A. Fedyanin, 2010, published in Pis'ma v Zhurnal Éksperimental'noĭ i Teoreticheskoĭ Fiziki, 2010, Vol. 92, No. 9, pp. 639–643.

Femtosecond Relaxation Dynamics of Surface Plasmon–Polaritons in the Vicinity of Fano-Type Resonance¶

P. P. Vabishchevich[a], V. O. Bessonov[a, b], F. Yu. Sychev[a], M. R. Shcherbakov[a], T. V. Dolgova[a], and A. A. Fedyanin[a]

[a] *Faculty of Physics, Moscow State University, Moscow, 119991 Russia*
e-mail: fedyanin@nanolab.phys.msu.ru

[b] *Frumkin Institute of Physical Chemistry and Electrochemistry, Russian Academy of Sciences, Moscow, 119991 Russia*

Received November 12, 2010

Temporal modification of femtosecond laser pulses reflected from planar periodic metal nanostructures with resonant excitation of surface plasmon–polaritons is experimentally studied. Spectral time-resolved measurements of the second-order cross-correlation function performed with the pulse duration comparable with the surface plasmon–polariton relaxation time (about 100 fs) show the strong spectral dependence of the envelope of the reflected femtosecond pulse described by Fano-resonance parameters.

DOI: 10.1134/S0021364010210022

Surface plasmon–polaritons (SPPs) are collective oscillations of electron plasma and electromagnetic field propagating along the metal-dielectric interface [1]. Recently, interest in investigations of SPPs has increased due to their possible use in the number of applications related to the light control at the microscopic scale. One of the ways to excite SPPs is to use periodically nanostructured metallic films, where new fascinating effects such as extraordinary optical transmission [2], negative refractive index [3, 4], and plasmon-induced optical birefringence and dichroism [5] have been recently found. Development of femtosecond lasers initiated the studies of the SPP temporal parameters [6–9]. Changes in the femtosecond pulse envelope were obtained for the pulses propagating through nanostructured metallic films due to SPP excitation [10–13]. A temporal delay of the femtosecond pulse passing through the nanostructured metallic film was found for the pulse wavelength close to the resonant one [10, 11]. Different SPP decay times at two band gap edges of plasmonic crystal has been demonstrated [13]. Spectral dependence of SPP-induced distortion of the femtosecond pulses has not been studied yet. Such measurements allow determination of dynamic parameters of SPP relaxation as well as optimal conditions for the control of SPP excitation at nanostructured metallic surfaces.

In this paper, temporal modification of femtosecond pulses upon the resonant excitation of surface plasmon–polaritons is studied in one-dimensional metallic nanogratings by femtosecond cross-correlation spectroscopy when the laser pulse duration is comparable with the SPP relaxation time. Modification reveals itself in the pulse duration changes and the pulse shift relative to the unperturbed pulse. Spectral dependence of the pulse distortion is described by the Fano resonance.

Samples are 50-nm silver films deposited on polymer substrates with a periodic surface topography fabricated by contact lithography. The atomic force microscopy image of the sample surface is shown in Fig. 1a and demonstrates the strict periodicity of sample topography and silver film homogeneity. Cross-section of the sample is close to sinusoidal profile with 750 nm-period and 60 nm-modulation depth. Optical reflection spectra are measured in the range of the angle of incidence θ from 16° to 70° with a step of 1° and in the wavelength range from 400 to 800 nm with a step of 1 nm. Frequency–angular measurements of reflectance spectra $R(\lambda, \theta)$ for the *p*-polarized radiation are represented in Fig. 2a. Three resonances caused by fulfillment of SPP phase-matching conditions at the silver–air interface by three diffraction orders, $n = +1$, -2, and -3 are observed: $k_{spp} = k_0 \sin\theta + ng$, where k_0 is the absolute value of the incident wave vector, k_{spp} is the absolute value of the SPP wave vector, and g is the absolute value of the reciprocal lattice vector. The frequency–angular dependences of the resonances are determined by the SPP dispersion law [1].

Figure 2b shows the reflection coefficient spectrum for *p*-polarized light at the angle of incidence of $\theta = 67°$, which is later used in the time-resolved experiments. Plasmonic origin of the resonance features observed in the vicinity of $\lambda = 500$ nm and $\lambda = 725$ nm is confirmed by the absence of such features in the reflection spectrum for *s*-polarization. Resonances

¶The article was translated by the authors.

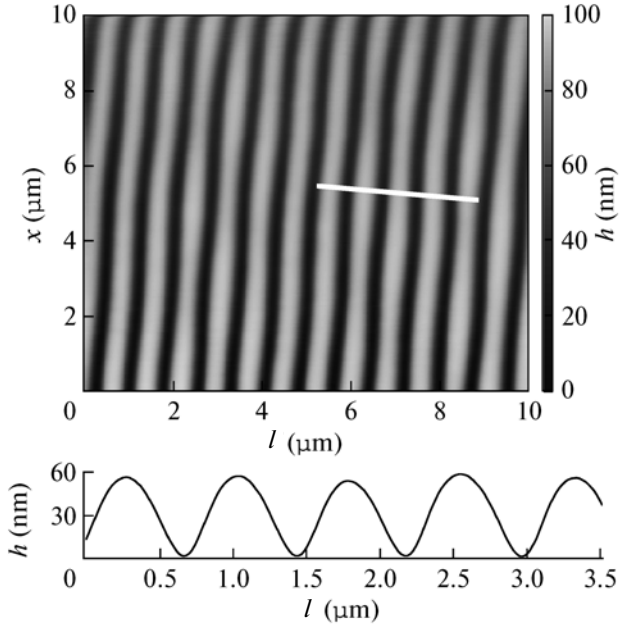

Fig. 1. (Upper panel) Atomic force microscopy image of the surface of the metallic nanograting. (Lower panel) Cross-section of the sample along the marked line.

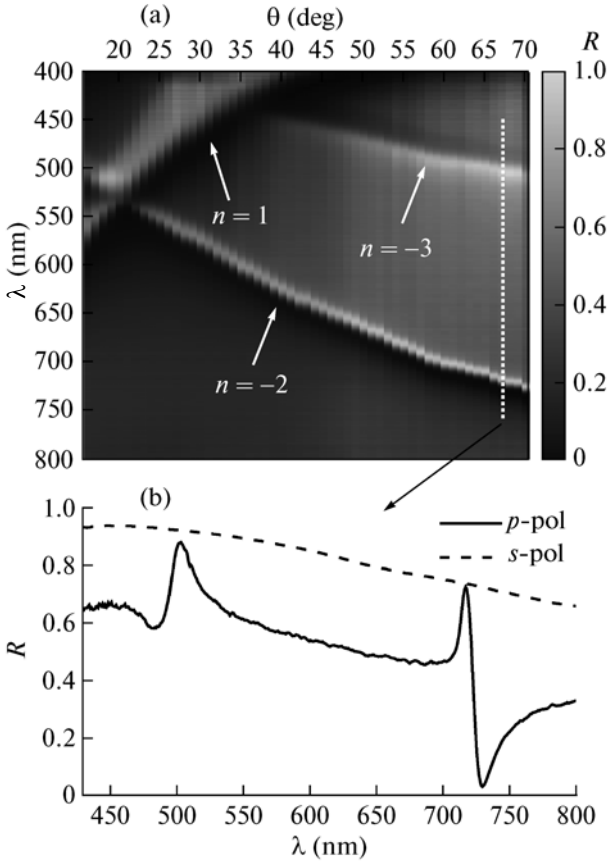

Fig. 2. (a) Reflection spectra of the metallic nanograting versus the angle of incidence measured for the *p*-polarized light; *n* is the diffraction order. (b) Spectra of the reflection coefficient for (solid line) *p*- and (dashed line) *s*-polarized light at $\theta = 67°$.

have Fano-type lineshapes [14, 15] caused by interference of the directly reflected light and reradiated SPP. The spectral line shape of the reflection coefficient $R(\omega) \equiv |r(\omega)|^2$ can be represented by a complex sum of the nonresonant reflection of incident radiation and the resonance profile of SPP with the Lorentzian lineshape:

$$r(\omega) = C_0 + \frac{f\Gamma e^{i\phi}}{\omega - \omega_R + i\Gamma}, \qquad (1)$$

where C_0 is the nonresonant reflection amplitude, ϕ is the phase difference between resonant and nonresonant components, f is the oscillator strength, ω_R is the Lorentz resonance frequency, and Γ is the SPP resonance width. The least-squares fit of Eq. (1) to the experimental dependence $R(\omega)$ measured for the *p*-polarized light (Fig. 2b) gives the following parameters of the long-wavelength resonance: $\lambda_R \equiv 2\pi c/\omega_R = 723 \pm 1$ nm, $\Gamma = (2.3 \pm 0.6) \times 10^{13}\ \mathrm{s}^{-1}$ ($\Delta\lambda \simeq 7$ nm). The SPP decay time calculated from the resonance width Γ is $t_{spp} \simeq 90$ fs.

The temporal modification of femtosecond pulses was studied by cross-correlation spectroscopy schematically shown in Fig. 3a. A Ti:sapphire laser with a pulse duration of approximately 200 fs, a repetition rate of 80 MHz, and the output wavelength tunable from 690 to 1020 nm was used as the radiation source. The average laser power on the sample was 100 mW. The laser pulse was divided at the beam splitter into two pulses, the first one is the reference pulse passing through the optical delay line and the second one is the signal pulse reflected from the sample. Both beams were then focused on the nonlinear BBO crystal, and noncollinear second-harmonic generation was detected by a photomultiplier tube (PMT). The angle of incidence of the laser radiation, θ, was chosen to overlap the spectral range of the plasmon resonance with the laser tuning range, in the experiment $\theta = 67°$. The experimental scheme allows measurements for both *p*- and *s*-polarized light. The dependence of the PMT signal on the delay time between pulses, τ, is the second-order cross-correlation function (CF) or, in other words, the cross-correlation function of the pulse intensity. The cross-correlation function of the *s*-polarized pulse is an autocorrelation function since there is no excitation of SPPs and the laser pulse reflects from the sample without any perturbation.

Measurements of the second-order cross-correlation function are performed in the spectral range from 710 to 800 nm in increment of 1 nm. Figure 3b shows the normalized cross-correlation function measured for *p*- and *s*-polarized light at resonant ($\lambda = 722$ nm)

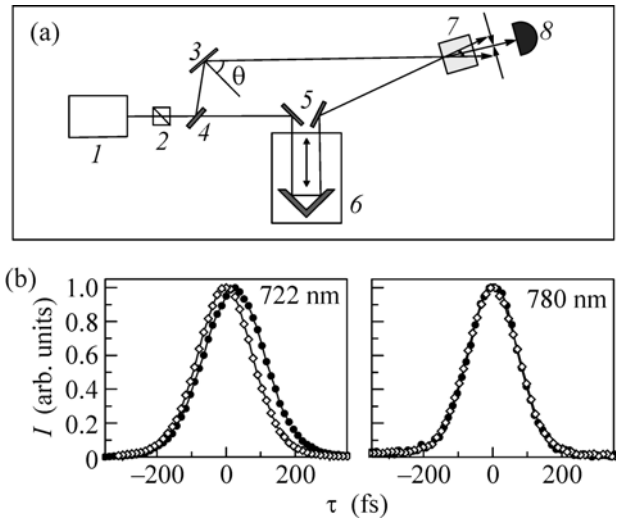

Fig. 3. (a) The femtosecond cross-correlation spectroscopy setup: (*1*) the Ti:sapphire laser, (*2*) the polarizer, (*3*) the sample, (*4*) the beam splitter, (*5*) the mirrors, (*6*) the optical delay line, (*7*) the BBO crystal, and (*8*) the photomultiplier tube. (b) Normalized second-order cross-correlation function in the case of (closed circles) *p*-polarization and (open circles) *s*-polarization measured at $\lambda =$ 722 and 780 nm; τ is the time delay between two pulses.

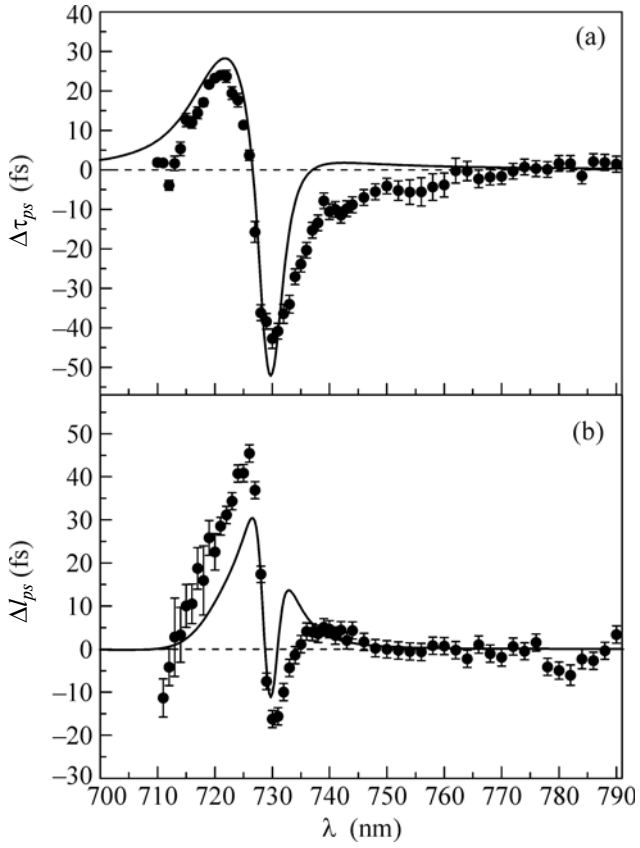

Fig. 4. Spectral dependences of the differences between the (a) positions, $\Delta\tau_{ps}$, and (b) widths, ΔI_{ps}, of the CF peaks. Points are the experimental data and lines are the numerical simulation results.

and nonresonant ($\lambda = 780$ nm) wavelengths. Pronounced modification of the CF shape and shift of the CF maximum are observed in the vicinity of the resonance for the *p*-polarized pulses relative to the *s*-polarized ones, while CF for the *p*- and *s*-polarized pulses measured far from the resonance are identical. The least-squares fit of the Gaussian function to experimental CF reveals CF maxima $\tau_p^{\max}$ and $\tau_s^{\max}$ and its FWHM $l_p^{\max}$ and $l_s^{\max}$ for *p*- and *s*-polarized pulses, respectively. Figure 4a shows spectral dependence of the time shift between CF maxima, $\Delta\tau_{ps} = \tau_p^{\max} - \tau_s^{\max}$. The reflected *p*-polarized pulse lags behind the *s*-polarized one in the spectral range of the central pulse wavelength from 713 to 726 nm with maximum CF delay being 24 ± 2 fs at $\lambda = 722$ nm. The latter is close to the resonant wavelength of $\lambda_R = 723 \pm 1$ nm obtained from the reflection spectrum fit (Fig. 2b). The *p*-polarized pulse gets ahead of the *s*-polarized one in the spectral region from 726 to 762 nm. The maximum $\Delta\tau_{ps}$ value is equal to 43 ± 2 fs at $\lambda = 730$ nm. Spectrum of the CF width difference, $\Delta l_{ps} = l_p^{\max} - l_s^{\max}$, is shown in Fig. 4b. The cross-correlation function of the *p*-polarized pulse is broadened in comparison with the *s*-polarized one for the central pulse wavelength from 713 to 728 nm. The maximum broadening is equal to 45 ± 2 fs at $\lambda = 726$ nm. Narrowing of CF of the *p*-polarized pulse is observed in the spectral region from 728 to 736 nm and its value is equal to 16 ± 2 fs at $\lambda = 730$ nm.

Broadening of CF measured for the *p*-polarized pulse and its delay in comparison with the nonresonance pulse is associated with the relaxation of resonantly excited surface plasmon–polaritons. The origin of the *p*-polarized pulse lag in the spectral range from 726 to 762 nm can be described within the following approach. In the vicinity of the Fano resonance minimum (730 nm) the CF amplitude measured for the *p*-polarized pulse and, consequently, intensity of the pulse reflected from the sample are smaller than that of the *s*-polarized pulse as it is shown in Fig. 5a. Asymmetry of the CF shape and the CF maximum shift are clearly seen. These are attributed to destructive interference between nonresonant and resonant reflected components of the *p*-polarized pulse as a result of additional phase difference between them appearing during the pulse wavelength tuning through the SPP resonance (Fig. 5b). If the pulse nonresonantly reflected from the sample is in-phase with the pulse resonantly reemitted due to SPP excitation, they interfere constructively leading to the CF maximum shift to the positive time scale and to the CF broaden-

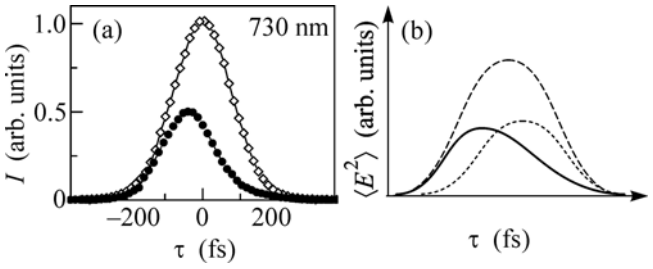

Fig. 5. (a) The second-order cross-correlation function for (closed circles) *p*-polarized and (open circles) *s*-polarized pulses at $\lambda = 730$ nm. (b) Schematic image of destructive interference between the (dashed line) nonresonant reflected component and (dotted line) delayed SPP excitation. The solid line shows resulting pulse reflected from the sample.

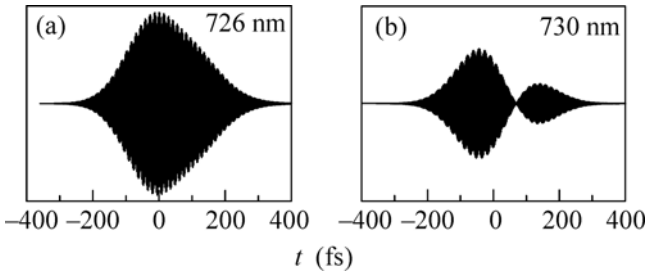

Fig. 6. Model time dependences of the electric field strength of the reflected pulse for (a) $\lambda = 726$ nm corresponding to the maximum CF broadening and (b) $\lambda = 730$ nm corresponding to the minimum of the Fano resonance.

ing. If pulses are in antiphase they interfere destructively that results in the CF peak shift to the negative direction and the CF narrowing. Far from the resonance as $\lambda > 750$ nm CF peaks and CF widths are almost identical for both pulse polarizations.

Let us consider $E_1(\omega)$ is the electric field strength of the reference pulse having a Gaussian form with the center frequency ω_0, the amplitude A_ω, and the pulse duration t_0:

$$E_1(\omega) = A_\omega e^{-\frac{1}{2}t_0^2(\omega-\omega_0)^2}. \quad (2)$$

In the time domain, it has the form

$$E_1(t) = Ae^{-t^2/2t_0^2}e^{-i\omega_0 t}. \quad (3)$$

Electric field strength $E_2(\omega)$ of the pulse reflected from the sample is expressed from Eq. (1) as:

$$E_2(\omega) = E_1(\omega)r(\omega) = A_\omega e^{-t_0^2(\omega-\omega_0)^2/2}\left(C_0 + \frac{fe^{i\phi}}{\omega-\omega_R+i\Gamma}\right). \quad (4)$$

In the time domain, according to the convolution theorem, the pulse has the form

$$E_2(t) = \int_{-\infty}^{+\infty} Ae^{-t'^2/2t_0^2}e^{-i\omega_0 t'} \times \left(f\Gamma e^{i\phi-(i\omega_R+\Gamma)(t-t')}H(t-t') + C_0\delta(t-t')\right)dt', \quad (5)$$

where $H(t)$ is the Heaviside step function. In the cross-correlation scheme, the E_2 pulse is spatially overlapped at the nonlinear crystal with the reference pulse, which is identical to the original E_1 pulse being delayed at τ. Measured second-harmonic intensity is proportional to the second-order cross-correlation function:

$$I_{\text{out}}(\tau) \sim \int_{-\infty}^{+\infty} |E_1(\tau-t')|^2 |E_2(t')|^2 dt' = \int_{-\infty}^{+\infty} I_1(\tau-t')I_2(t')dt'. \quad (6)$$

Numerical simulation of the cross-correlation functions is carried out by using Eqs. (3)–(6) with the following parameters extracted from the fit of the experimental reflection spectrum (Fig. 2b): $\omega_R = 2.61 \times 10^{15}$ s^{-1} ($\lambda_R = 723$ nm); $\Gamma = 2.3 \times 10^{13}$ s^{-1}; $f = 0.74$; $\phi = 0.22\pi$; $A = 1$; $C_0 = 0.63$; $t_0 = 200$ fs. Calculated spectral dependences of the CF maximum shift $\Delta\tau_{ps}$ and the CF width difference Δl_{ps} are shown by lines in Fig. 4. The model lines are in good agreement with the experimental dependences $\Delta\tau_{ps}(\lambda)$ and $\Delta l_{ps}(\lambda)$; for this reason, the electric field strength $E_2(t)$ of the pulse reflected from the sample can be reconstructed: the results are shown in Fig. 6. For $\lambda = 726$ nm corresponding to the maximum CF broadening, $E_2(t)$ is broadened relative to the reference pulse due to the SPP excitation (Fig. 6a). Significant changes of the $E_2(t)$ profile are also observed at the Fano resonance minimum at $\lambda = 730$ nm (Fig. 6b) as the resonant component of the reflected pulse is in antiphase with the nonresonant one producing the local minimum of $E_2(t)$. Control of plasmonic optical response of nanostructures, its amplification or suppression at the desired time moment is realizable if $t_0 \sim t_{\text{spp}}$. It is impossible either for ultrashort laser pulses, $t_0 \ll t_{\text{spp}}$, as optical response is defined by the reradiated plasmon–polariton or for continuous pumping, $t_0 \gg t_{\text{spp}}$, as the nonresonantly reflected radiation dominates in the response.

In conclusion, noticeable temporal distortion of the femtosecond laser pulses reflected from the one-dimensional metallic nanograting is observed. The

pulse modification occurs due to resonant excitation of the surface plasmon–polaritons with decay time comparable with the pulse duration and manifests itself in the maximum shift and the width changes of the second-order cross-correlation function. Spectral behavior of the pulse shape changes is governed by the femtosecond SPP relaxation dynamics described by the Fano-type resonance. Both a decrease and an increase in the reflected pulse duration are found. Leading and delaying of the pulse reflected from the sample relative to the unperturbed pulse are found to be up to 24 ± 2 fs and 43 ± 2 fs, respectively, for the pulse width $t_0 \simeq 200$ fs and SPP time decay $t_{spp} \simeq 90$ fs.

This work was supported by the Russian Foundation for Basic Research, project nos. 10-02-91170 and 10-02-92115, and by the Ministry of Education and Science of the Russian Federation, contract nos. P918, P946, and P1465. We are grateful to E.D. Mishina (Moscow State Institute of Radio Engineering, Electronics, and Automation) for fruitful discussions and access to femtosecond laser facilities.

REFERENCES

1. H. Raether, *Surface Plasmons on Smooth and Rough Surfaces and Gratings*, Springer Tracts on Modern Physics, Vol. 111 (Springer, New York, 1988).
2. T. W. Ebbesen, H. J. Lezec, H. F. Ghaemi, et al., Nature **391**, 667 (1998).
3. V. G. Veselago, Usp. Fiz. Nauk **92**, 517 (1967) [Sov. Phys. Usp. **10**, 509 (1968)].
4. R. Shelby, D. Smith, and S. Schultz, Science **292**, 77 (2001).
5. M. R. Shcherbakov, P. P. Vabishchevich, M. I. Dobynde, et al., Pis'ma Zh. Eksp. Teor. Fiz. **90**, 478 (2009) [JETP Lett. **90**, 433 (2009)].
6. N. Rotenberg, M. Betz, and H. M. van Driel, Opt. Lett. **33**, 2137 (2008).
7. A. Kubo, N. Pontius, and H. Petek, Nano Lett. **7**, 470 (2007).
8. M. Tong, A. S. Kirakosyan, T. V. Shahbazyan, et al., Phys. Rev. Lett. **100**, 056808 (2008).
9. Yu. E. Lozovik, S. P. Merkulova, M. M. Nazarov, et al., Phys. Lett. A **276**, 127 (2000).
10. A. Dogariu, T. Thio, and L. J. Wang, Opt. Lett. **26**, 450 (2001).
11. D. S. Kim, S. C. Hohng, V. Malyarchuk, et al., Phys. Rev. Lett. **91**, 143901 (2003).
12. C. Ropers, D. J. Park, G. Stibenz, et al., Phys. Rev. Lett. **94**, 113901 (2005).
13. A. S. Vengurlekar, A. V. Gopal, and T. Ishihara, Appl. Phys. Lett. **89**, 181927 (2006).
14. U. Fano, Ann. Phys. **32**, 393 (1938).
15. C. Genet, M. P. van Exter, and J. P. Woerdman, Opt. Commun. **225**, 331 (2003).